Flow, slippage and a hydrodynamic boundary condition of polymers at surfaces

2008 J. Phys.: Condens. Matter 20 494225

(http://iopscience.iop.org/0953-8984/20/49/494225)

J. Phys.: Condens. Matter **20** (2008) 494225 (6pp) doi:10.1088/0953-8984/20/49/494225

Flow, slippage and a hydrodynamic boundary condition of polymers at surfaces

M Müller[1], C Pastorino[1,2] and J Servantie[1]

[1] Institut für Theoretische Physik, Georg-August-Universität, D-37077 Göttingen, Germany
[2] Departamento de Física, Centro Atómico Constituyentes, CNEA-CONICET, 1650 San Martín, Pcia de Buenos Aires, Argentina

E-mail: mmueller@theorie.physik.uni-goettingen.de

Received 4 July 2008, in final form 22 July 2008
Published 12 November 2008
Online at stacks.iop.org/JPhysCM/20/494225

Abstract

Tailoring surface interactions or grafting of polymers onto surfaces is a versatile tool for controlling wettability, lubrication, adhesion and interactions between surfaces. Using molecular dynamics of a coarse-grained, bead-spring model and dynamic single-chain-in-mean-field simulations, we investigate how structural changes near the surface affect the flow of a polymer melt over the surface and how these changes can be parameterized by a hydrodynamic boundary condition.

We study the temperature dependence of the near-surface flow of a polymer melt at a corrugated, attractive surface. At weakly attractive surfaces, lubrication layers form, the slip length is large and increases upon cooling. Close to the glass transition temperature, very large slip lengths are observed. At a more attractive surface, a 'sticky surface layer' is build up, giving rise to a small slip length. Upon cooling, the slip length decreases at high temperatures, passes through a minimum and increases upon approaching the glass transition temperature. At strongly attractive surfaces, the Navier slip condition fails to describe Couette and Poiseuille flows simultaneously.

A similar failure of the Navier slip condition is observed for the flow of a polymer melt over a brush comprised of identical molecules. The wetting and flow properties of this surface are rather complex. Most notably, the cyclic motion of the grafted molecules gives rise to a reversal of the flow direction at the grafting surface.

The failure of the Navier slip condition in both cases can be rationalized within a schematic, two-layer model, which demonstrates that the Navier slip condition fails to simultaneously describe Poiseuille and Couette flow if the fluid at the surface exhibits a higher viscosity than the bulk.

(Some figures in this article are in colour only in the electronic version)

1. Introduction

The equilibrium and flow properties of fluids at surfaces have attracted abiding interest [1, 2]. Due to the large area-to-volume ratio in nano- and microfluidic devices, the properties of the confining boundaries influence the flow behavior. Commonly, the effect of surfaces enters the macroscopic hydrodynamic description via the Navier–Stokes equation as a boundary condition. This hydrodynamic boundary condition [3] describes the molecular structure and dynamics at the surface by a few parameters, i.e. slip length, δ, and boundary position, x_b. These parameters are independent of the type and strength of flow but they are a material property of the surface.

The equilibrium properties of a liquid drop on a surface are dictated by the balance of surface and interface tensions. Young's equation [4]:

$$\gamma_{LV} \cos\Theta + \gamma_{LW} = \gamma_{VW} \quad (1)$$

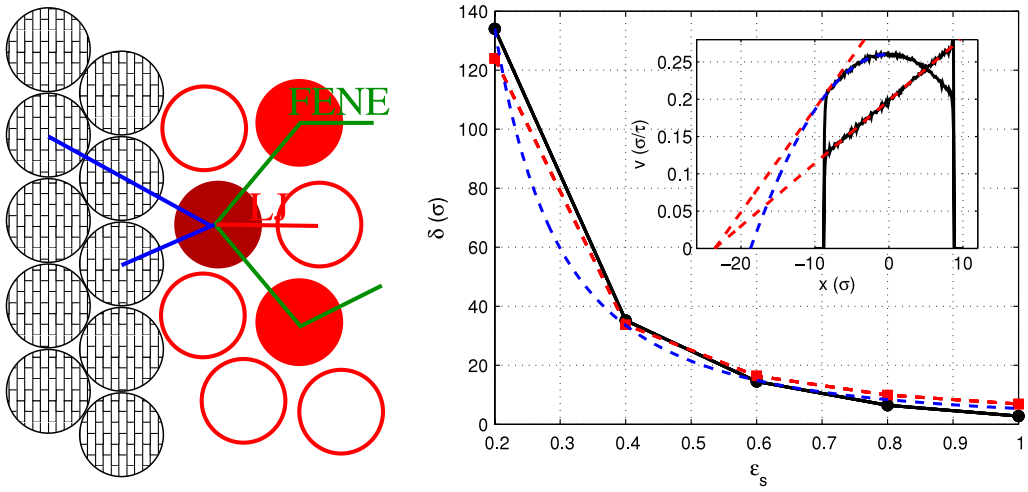

Figure 1. (a) Sketch of the interactions in our coarse-grained model of a polymer liquid in contact with a solid substrate. (b) Slip length, δ, as a function of the attraction strength, ϵ_S, between solid and liquid for temperature, $k_BT/\epsilon = 1.2$. The solid line with circles is obtained from the Couette and Poiseuille profiles while the dashed line with squares is from the Green–Kubo relation (3). The curve marks the behavior $\delta \sim 1/\epsilon_S^2$. The inset illustrates the velocity profiles of Couette and Poiseuille flows, from which the slip length has been estimated for $\epsilon_S = 0.6$, measured in units of the Lennard-Jones parameter, ϵ. Adapted from [8].

expresses the macroscopic contact angle, Θ, a drop makes with the surface as a function of the tension of the liquid–vapor interface, γ_{LV} and the surface tensions of the liquid and the vapor, γ_{LW} and γ_{VW} with the solid substrate. An analogue balance of stresses at the surface:

$$\eta \left.\frac{\partial v_\parallel(x)}{\partial x}\right|_{x_b} = \lambda v_\parallel(x)|_{x_b} \tag{2}$$

characterizes the Navier slip condition [3], which states the equilibrium of viscous stress in the fluid and the friction stress at the substrate at a position, x_b. η denotes the viscosity of the liquid and λ is the friction coefficient. The latter can be obtained via a Green–Kubo formula by integrating the autocorrelation function of the tangential force, $\mathbf{F}_\parallel$, exerted by the wall on the fluid [5, 6]:

$$\lambda = \frac{1}{k_BTA}\int_0^\infty \mathrm{d}t\, \langle \mathbf{F}_\parallel(t)\mathbf{F}_\parallel(0)\rangle \tag{3}$$

where A denotes the surface area. The ratio $\delta \equiv \eta/\lambda$ defines the slip length.

At soft, deformable surfaces (like polymer brushes or networks) or if the molecular properties are altered in the vicinity of the surface, the position, x_b, at which the boundary condition is to be enforced is not obvious and may change with temperature or other external control parameters (e.g. grafting density, σ_{brush}, of the brush). In this case, the two parameters of the Navier slip condition have to be extracted from two independent flow profiles.

In this paper, we use Couette and Poiseuille flows in a channel of width, D. At the center of the channel, the flow is described by the Navier–Stokes equation, yielding a linear velocity profile with shear rate, $\dot\gamma$ [7]:

$$v_{\mathrm{hydro,C}}(x) = \dot\gamma\,(x - x_C) \tag{4}$$

for Couette flow and a parabolic one:

$$v_{\mathrm{hydro,P}}(x) = \frac{g_\parallel}{2\eta}\,(x - x_P)\,(D - x_P - x) \tag{5}$$

for Poiseuille flow. $g_\parallel$ characterizes the body force (e.g. gravity) acting on the fluid. x_C and x_P denote the positions where the hydrodynamic velocity profiles extrapolate to zero. From these two quantities, one obtains the slip length, δ, and the position of the hydrodynamic boundary, x_b, according to

$$\delta = \sqrt{(x_P - x_C)(D - x_P - x_C)} \tag{6}$$

$$x_b = x_C + \delta. \tag{7}$$

Much effort has been directed towards tailoring surface properties by coatings. Molecular simulations are well suited to investigate how changes of the molecular conformations at surfaces, adsorption layers or irreversibly bound molecules (brushes) influence the surface free energy and stress. The interplay between the structural and dynamic properties on the molecular scale and the macroscopic description is incompletely understood. The molecular information enters into the macroscopic description in the form of a boundary condition. Computing the parameters of the boundary condition via molecular simulation is a first step towards a multi-scale modeling of microfluidic devices from the molecular structure to the length scale of micrometers.

2. Model and techniques

We investigate the flow of a dense polymer melt over a hard, solid substrate and a polymer brush. The first system is studied by molecular dynamics simulations of a coarse-grained bead-spring model, which is sketched in figure 1(a). Segments interact via a Lennard-Jones potential with a range, $r_c = 2\sqrt[6]{2}\sigma$, where σ denotes the diameter of a bead. Polymers

are comprised of $N = 10$ segments. Neighboring segments along the polymer are bonded via a FENE potential [9]. The model exhibits a glass transition around $k_BT/\epsilon \approx 0.4$ [10], where k_B denotes Boltzmann's constant and ϵ is the energy parameter of the Lennard-Jones potential. The phase behavior and wetting properties as well as the dynamics in the bulk and in confinement have been recently reviewed [11, 10]. The equations of motions are integrated using the velocity-verlet algorithm. A dissipative particle dynamics (DPD) thermostat [12, 13] is used to control temperature, T, and the density, ρ, inside the film corresponds to the liquid–vapor coexistence [14, 15]. The film surface is modeled by two rigid layers of Lennard-Jones interaction centers arranged on an FCC lattice. Further details about the model can be found in [8]. By varying the strength, ϵ_S, of the Lennard-Jones potential between solid and fluid, we tune adhesion, wettability and slip.

Figure 1(b) presents the slip length, δ, as a function of the solid–liquid attraction, ϵ_S, at high temperature, $k_BT/\epsilon = 1.2$. The Green–Kubo formula (3) as well as the combination of Poiseuille and Couette flows yield consistent results. In accordance with expectation, the slip length is smaller the larger is the solid–liquid attraction, ϵ_S.

The flow over polymer brushes is investigated by dynamic single-chain-in-mean-field (SCMF) simulations [16, 17], which describe the motion of polymer molecules in a self-consistently determined flow field. In SCMF simulations [16, 17] one considers a large ensemble of explicit chain configurations that independently evolve in an external field, W. This field mimics the effect of the non-bonded interactions (i.e. repulsion of segments in a dense melt) and its gradient gives rise to a force, $\mathbf{F}_{nb}$. Chain segments evolve via smart Monte Carlo (SMC) moves [18, 19] with trial displacements:

$$\Delta\mathbf{r}_{trial} = (\zeta\langle\bar{\mathbf{v}}\rangle + \mathbf{F})\,\Delta t/\zeta + \xi\sqrt{2k_BT\,\Delta t/\zeta}. \qquad (8)$$

$\mathbf{F}$ denotes the force acting on a segment, which comprises contributions from bonding forces, the non-bonded repulsion between segments and interactions with the confining boundaries. ζ characterizes the segmental friction and ξ is a Gaussian random number with zero mean and unit variance. We set $\zeta N = 1$. $\langle\bar{\mathbf{v}}(\mathbf{r})\rangle$ denotes the hydrodynamic velocity field. Chains exhibit Rouse-like dynamics characteristic for unentangled melts [20] and the Weissenberg number is defined as $Wi \equiv \dot{\gamma}\zeta N R_e^2/(3\pi^2 k_BT)$, where $\dot{\gamma}$ denotes the shear rate and R_e is the end-to-end distance of the polymers. The fluctuating, external field, W, is calculated from the densities after every time step, and the densities are constructed by assigning the instantaneous particle positions to a three-dimensional grid with linear spacing $\Delta L = R_e/6$ [17]. The hydrodynamic velocity, $\langle\bar{\mathbf{v}}\rangle$, however, represents the average flow field and must not fluctuate. First, we directly calculate an instantaneous velocity, $\mathbf{v}_i = \Delta\mathbf{r}_i/\Delta t$, of segment i from its explicit displacement [21] during an SMC step (in order to retain spatial resolution) and assign it to the grid. Then, we add the instantaneous velocities of all segments, average over a time period, $\bar{t}$, and normalize by the local density to obtain the average local velocity $\langle\bar{\mathbf{v}}(\mathbf{r})\rangle$. This procedure ensures that the average force, $\langle\bar{\mathbf{F}}\rangle$, vanishes. This time averaging procedure limits the simulation technique to stationary or slowly varying flows. For the density utilized in our simulations a time interval $\bar{t} \geqslant 800\zeta R_e^2/(Nk_BT)$ is sufficient to eliminate fluctuations of the velocity field and to yield accurate predictions in equilibrium.

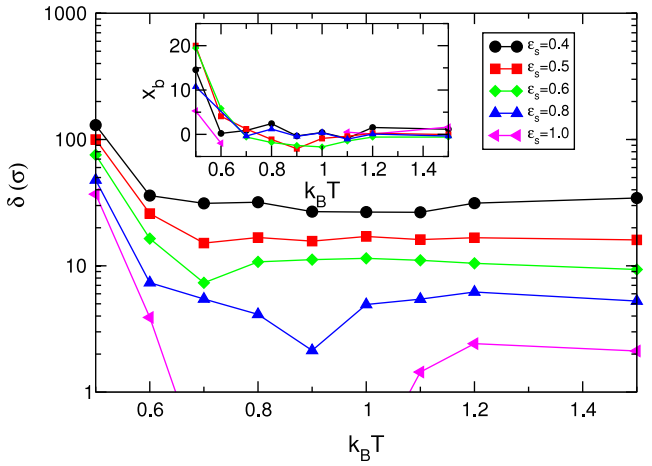

Figure 2. Slip length, δ, versus temperature for different strengths, ϵ_S, of solid–fluid interaction. The inset represents the position of the hydrodynamic boundary, x_b, versus temperature. All lengths, δ and x_b, are measured in units of the Lennard-Jones parameter, σ, and the thermal energy, k_BT, in units of the Lennard-Jones parameter, ϵ. Adapted from [23].

The dynamic SCMF simulation method is computationally efficient and allows us to study dense polymer systems under weak flow. Additional details of the simulation method can be found in [7]. The results have been corroborated by extensive molecular dynamics simulations [22, 13] using similar techniques as for the flow over solid substrates.

3. Results

3.1. Molecular simulations

3.1.1. Polymer melt at an attractive surface. Using Poiseuille and Couette flows, we have extracted δ and x_b for the flow of a polymer melt over an attractive solid. The results for the slip length are presented in figure 2 and the location of the hydrodynamic boundary, x_b, is depicted in the inset. We see that the temperature dependence of δ is highly sensitive to temperature and solid–fluid interaction. First, we observe that, independent of ϵ_S, the slip length diverges as we approach the glass transition temperature, T_g, because the fluid eventually behaves like a solid. Already at $k_BT/\epsilon = 0.5$, i.e. about 20% above the glass transition temperature of our model, δ has increased by an order of magnitude compared to the approximately constant value at high temperature. This observation offers an explanation for the surprisingly large slip length observed in the dewetting experiment of Fetzer *et al* [24], which was performed in the vicinity of the glass transition temperature.

Within the accuracy of our simulations, x_b does not vary significantly with the strength of the fluid–solid interaction

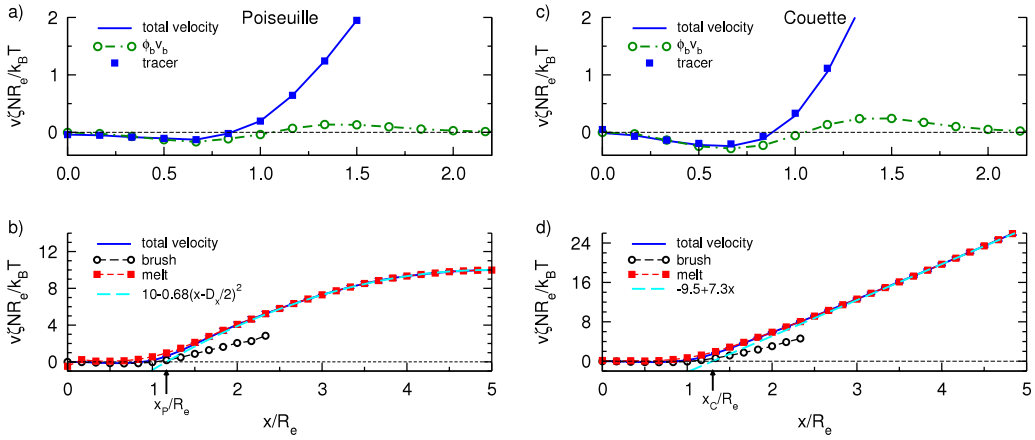

Figure 3. Mass averaged, total velocity profile, $\langle \bar{v}_\parallel \rangle$, and velocity of brush and melt segments for Poiseuille ((a) and (b)) and Couette ((c) and (d)) flows. Panels (a) and (c) highlight the total velocity at the surface and show details of $\phi_{\text{brush}} v_{\text{brush}}$. Additionally, the velocity profiles of tracer particles, which have the same extension and mass as the segments of brush or melt polymers but a large friction, are depicted. Their velocity coincides with the fluid velocity. Panels (b) and (d) display the velocity profiles across half of the film. The dashed line is a fit to macroscopic predictions (cf equations (5) and (4)). The arrow marks the positions, x_P and x_C, at which the extrapolation of the macroscopic hydrodynamic velocity profile vanishes. Adapted from [7].

over the entire temperature regime. At high temperature, x_b is close to the top of the solid substrate, while it gradually shifts inwards as the temperature is reduced towards T_g. This effect goes along with a growing distance over which the liquid structure is altered by the surface, as can be observed, for instance, in the pronounced packing effects in the density profile.

The qualitative behavior of δ depends on the strength of the solid–fluid interaction. While δ monotonically decreases with temperature for $\epsilon_S = 0.4$ and 0.5 (measured in units of ϵ), we observe a non-monotonic variation of δ for larger solid–liquid attraction. For very strong attraction, $\epsilon_S = 1$, there is even a region of intermediate temperatures where $x_C < x_P$ and thus equation (6) has no solution. This marks the failure of the Navier slip condition to parameterize the near-surface flow solely by the material properties of the solid surface.

3.1.2. Flow at the brush–melt interface. The velocity profiles of Couette and Poiseuille flows over a polymer brush that is comprised of identical molecules as the melt is presented in figure 3. For the grafting density studied, $\sigma_{\text{brush}} R_e^2/\sqrt{\bar{N}} = 1$ with $\bar{N} = (\rho R_e^3/N)^2 = 128^2$, there is a broad interface between brush and melt. This system is an example of a soft surface with a complex wetting behavior [25, 26] and rich flow behavior [27, 22]. For these complex surfaces, the location of the hydrodynamic boundary, x_b, depends on the grafting density and interdigitation of brush and melt. Moreover, the molecules of the brush perform a tumbling motion [7], similar to what has been observed for isolated molecules grafted to a surface in shear flow [28–31]. The collective behavior of the brush chains leads to a reversal of the total flow direction inside the brush. Some aspects of this behavior are illustrated in panels (a) and (c), and the phenomenon has also been confirmed by molecular dynamics simulations [7]. We note that the effect of the brush on the flow of the melt cannot be captured by modeling the brush as a porous medium [32, 33]; an explicit description of the homopolymer solvent is required.

The lower panels of figure 3 depict the flow velocity profiles across the channel and fits to the hydrodynamic predictions (5) and (4) that describe the flow at the center. Similar to the behavior of a polymer melt at a strongly attractive surface, we observe $x_P < x_C$ and conclude that the Navier slip condition does not provide a consistent boundary condition.

3.2. Schematic, two-layer model

In order to rationalize these simulation results and explore whether they are universal, we propose a schematic two-layer model depicted in figure 4. Within this model, we approximate the gradual variation of the fluid properties as a function of the distance from the solid surface by a boundary region of width, Δ, which is characterized by a surface viscosity, η_S. Within each layer, surface layer and bulk, the fluid is described by the Navier–Stokes equation. At the interface between the solid substrate and the surface layer, we impose a Navier slip condition (2) with a microscopic slip length, δ_S, at the origin, $x = 0$. At the interface between the surface layer and bulk region, we require the continuity of shear stress and velocity:

$$\eta_S \left.\frac{\partial v}{\partial x}\right|_{x=\Delta^-} = \eta \left.\frac{\partial v}{\partial x}\right|_{x=\Delta^+} \qquad \text{and} \qquad v|_{x=\Delta^-} = v|_{x=\Delta^+}. \tag{9}$$

One can straightforwardly calculate the flow profiles at the surface and in the bulk. For Couette flow, one obtains

$$v = \dot{\gamma} \frac{\eta}{\eta_S}(x - \delta_S) \qquad \text{for } x < \Delta \tag{10}$$

$$v = \dot{\gamma}\,(x - x_C) \qquad \text{for } x \geqslant \Delta$$

$$\text{with } x_C = \left(1 - \frac{\eta}{\eta_S}\right)\Delta - \frac{\eta}{\eta_S}\delta_S \tag{11}$$

A similar calculation yields

$$v = -\frac{g_\parallel}{2\eta_S}\left(x^2 - Dx - D\delta_S\right) \qquad \text{for } x < \Delta \tag{12}$$

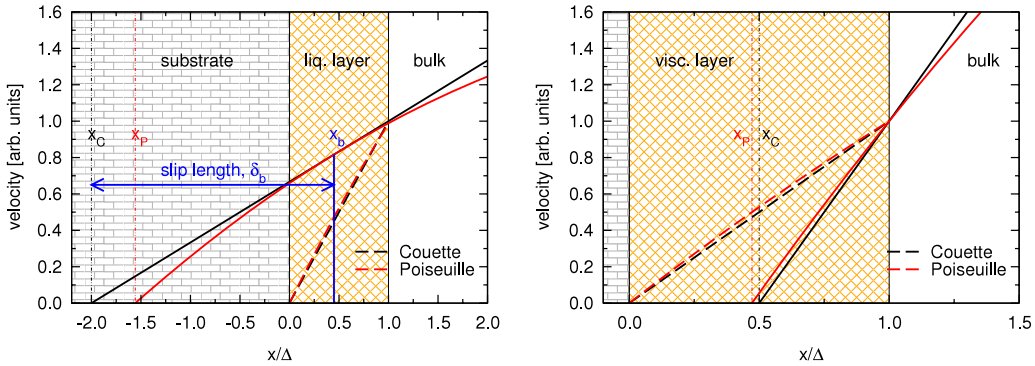

Figure 4. Couette and Poiseuille flow profiles at a two-layer surface for the special case of a microscopic no-slip boundary ($\delta_S = 0$) and a channel of width $D = 10\Delta$. In (a) the boundary layer has a lower viscosity, $\eta_S = \eta/3$, than the bulk. Dashed lines show the velocity profile inside the layer; solid lines represent the flow at the center and its continuation inside the boundary layer. This continuation vanishes at x_C or x_P for Couette and Poiseuille flow, respectively. The position, x_b, at which the hydrodynamic boundary condition should be applied and the slip length, δ_b, are indicated. Panel (b) depicts the case where the boundary layer has a higher viscosity, $\eta_S = 2\eta$, and the Navier slip condition cannot simultaneously describe both flows because $x_P < x_C$.

$$v = \frac{g_\parallel}{2\eta}(x - x_P)(D - x_P - x) \qquad \text{for } x \geqslant \Delta$$

$$\text{with } x_P(D - x_P) = -\left(1 - \frac{\eta}{\eta_S}\right)\Delta^2 + Dx_C \tag{13}$$

for Poiseuille flow. D denotes the film thickness, which is defined by the distance between the positions where the microscopic Navier slip condition with slip length, δ_S, is applied.

Finally, equation (6) yields the slip length

$$\delta = \sqrt{\Delta\frac{\eta}{\eta_S}\left(\frac{\eta}{\eta_S} - 1\right)(\Delta + 2\delta_S) + \left(\frac{\eta}{\eta_S}\delta_S\right)^2}. \tag{14}$$

The first term describes the effect of the surface layer, while the second term arises from the microscopic slip at the solid surface. For surfaces with a large surface mobility, $\eta/\eta_S > 1$, a lubrication layer is formed and results in an enhanced slip length, $\delta > \delta_S$, compared to the microscopic slip at the solid–fluid interface. On the other hand, if the solid–fluid interactions give rise to a boundary layer with large effective viscosity, $\eta/\eta_S < 1$, the presence of this sticky layer at the substrate reduces the slip length, $\delta < \delta_S$. Moreover, if

$$\frac{\eta}{\eta_S} \leqslant \frac{1 + 2\delta_S/\Delta}{(1 + \delta_S/\Delta)^2} \tag{15}$$

the velocity far away from the surface cannot be described by the Navier–Stokes equation and a Navier slip condition (2).

This schematic model can rationalize the observations in our molecular simulation: (i) at high temperature, kinetic effects will dominate the behavior, thus $\eta_S \approx \eta$. In this case, δ is equal to the microscopic slip length $\delta \approx \delta_S$. (ii) Upon cooling the fluid, the bulk viscosity increases. If the solid–fluid interactions are weak, $\epsilon_S < 0.5$, a lubrication layer is formed and the slip length increases, $\delta \propto (\eta/\eta_S)(\Delta + \delta_S)$. (iii) If the coupling between solid and fluid is strong or the near-surface viscosity is enhanced due to the brush coating, however, the ratio η/η_S decreases upon cooling and so does δ. If the ratio becomes sufficiently small (cf equation (15)), as it does in the case $\epsilon_S = 1$ for a melt at an attractive surface or for a brush-coated surface, the Navier slip condition fails. Upon approaching T_g from above, however, the slip length passes through a minimum and increases. The latter effect stems from the temperature dependence of the microscopic slip length, $\delta_S = \eta_S/\lambda$, which diverges for $T \to T_g$.

4. Discussion

We have investigated the hydrodynamic boundary condition of a polymer liquid over solid and soft surfaces by molecular dynamics and dynamic single-chain-in-mean-field simulations. If the near-surface viscosity is lower than the bulk viscosity, the effect of this lubrication layer can consistently be described by the Navier slip condition. In contrast, if the surface interactions lead to the formation of a 'sticky' surface layer, which is characterized by a higher viscosity than the bulk, the Navier slip condition will fail to describe Poiseuille and Couette flows simultaneously. The findings of the molecular simulations can be rationalized by a schematic, two-layer model. While this two-layer model provides a description for the examples discussed in this paper, alternatives that may substitute for the Navier slip condition remain to be explored.

Acknowledgments

It is great pleasure to thank K Binder, K Ch Daoulas and M P Allen for fruitful discussions. Financial support by DFG-priority program 'nano- and microfluidics' (Mu1674/3), the EU-project INFLUS (NMP-031980), the DAAD and the Volkswagen Foundation are gratefully acknowledged. Ample computer time has been provided by the Jülich Supercomputer Center and the GWDG, Göttingen.

References

[1] Tabelling P 2006 *Introduction to Microfluidics* (Oxford: Oxford University Press)
[2] Squires T M and Quake S R 2005 Microfluidics: fluid physics at the nanoliter scale *Rev. Mod. Phys.* **77** 977–1026
[3] Navier C L M H 1823 Sur les lois du mouvement des fluides *Mem. Acad. R. Sci. Inst. France* **6** 389–440

[4] Young T 1805 *Phil. Trans. R. Soc.* **5** 65
[5] Bocquet L and Barrat J-L 1993 Hydrodynamic boundary conditions and correlation functions of confined fluids *Phys. Rev. Lett.* **70** 2726
[6] Bocquet L and Barrat J-L 1994 Hydrodynamic boundary conditions, correlation functions, and kubo relations for confined fluids *Phys. Rev.* E **49** 3079
[7] Müller M and Pastorino C 2008 Cyclic motion and inversion of surface flow direction in a dense polymer brush under shear *Europhys. Lett.* **81** 28002
[8] Servantie J and Müller M 2008 Statics and dynamics of a cylindrical droplet under an external body force *J. Chem. Phys.* **128** 014709
[9] Grest G S and Kremer K 1986 Molecular dynamics simulations for polymers in the presence of a heat bath *Phys. Rev.* A **33** 3628
[10] Baschnagel J and Varnik F 2005 Computer simulations of supercooled polymer melts in the bulk and in-confined geometry *J. Phys.: Condens. Matter* **17** R851–953
[11] Müller M and MacDowell L G 2003 Wetting of polymer liquids: Monte Carlo simulations and self-consistent field calculations *J. Phys.: Condens. Matter* **15** R609–53
[12] Hoogerbrugge P J and Koelman J M V A 1992 Simulating microscopic hydrodynamics phenomena with dissipative particle dynamics *Europhys. Lett.* **19** 155
[13] Pastorino C, Kreer T, Müller M and Binder K 2007 Comparison of dissipative particle dynamics and langevin thermostats for out-of-equilibrium simulations of polymeric systems *Phys. Rev.* E **76** 026706
[14] Müller M and MacDowell L G 2000 Interface and surface properties of short polymers in solution: Monte Carlo simulations and self-consistent field theory *Macromolecules* **33** 3902–23
[15] Müller M, MacDowell L G and Yethiraj A 2003 Short chains at surfaces and interfaces: a quantitative comparison between density-functional theories and Monte Carlo simulations *J. Chem. Phys.* **118** 2929–40
[16] Müller M and Smith G D 2005 Phase separation in binary mixtures containing polymers: a quantitative comparison of single-chain-in-mean-field simulations and computer simulations of the corresponding multichain systems *J. Polym. Sci.* B **43** 934–58
[17] Daoulas K Ch and Müller M 2006 Single-chain-in-mean-field simulations: quasi-instantaneous field approximation and quantitative comparison with Monte Carlo simulations *J. Chem. Phys.* **125** 184904
[18] Rossky P J, Doll J D and Friedman H L 1978 Brownian dynamics as smart Monte Carlo simulation *J. Chem. Phys.* **69** 4628–33
[19] Allen M and Tildesley D 1987 *Computer Simulation of Liquids* (Oxford: Clarendon)
[20] Doi M and Edwards S F 1994 *The Theory of Polymer Dynamics* (Oxford: Oxford University Press)
[21] Narayanan B and Ganesan V 2006 Flow deformation of polymer blend droplets and the role of block copolymer compatibilizers *Phys. Fluids* **18** 042109
[22] Pastorino C, Binder K, Kreer T and Müller M 2006 Static and dynamic properties of the interface between a polymer brush and a melt of identical chains *J. Chem. Phys.* **124** 064902
[23] Servantie J and Müller M 2008 Temperature dependence of the slip length in polymer melts at attractive surfaces *Phys. Rev. Lett.* **101** 026101
[24] Fetzer R, Rauscher M, Münch A, Wagner B A and Jacobs K 2006 Slip-controlled thin-film dynamics *Europhys. Lett.* **75** 638–44
[25] Müller M and MacDowell L G 2001 Wetting of a short chain liquid on a brush: first-order and critical wetting transitions *Europhys. Lett.* **55** 221–7
[26] MacDowell L G and Müller M 2006 Adsorption of polymers on a brush: tuning the order of the wetting phase transition *J. Chem. Phys.* **124** 084907
[27] Doyle P S, Shaqfeh E S G and Gast A P 1997 Dynamic simulation of freely draining flexible polymers in steady linear flows *J. Fluid Mech.* **334** 251–91
[28] Doyle P S, Ladoux B and Viovy J L 2000 Dynamics of a tethered polymer in shear flow *Phys. Rev. Lett.* **84** 4769–72
[29] Gerashchenko S and Steinberg V 2006 Statistics of tumbling of a single polymer molecule in shear flow *Phys. Rev. Lett.* **96** 038304
[30] Delgado-Buscalioni R 2006 Cyclic motion of a grafted polymer under shear flow *Phys. Rev. Lett.* **96** 088303
[31] Winkler R G 2006 Semiflexible polymers in shear flow *Phys. Rev. Lett.* **97** 128301
[32] Milner S T 1991 Hydrodynamic penetration into parabolic brushes *Macromolecules* **24** 3704–5
[33] Brinkman H C 1947 A calculation of the viscous force exerted by a flowing fluid on a dense swarm of particles *Appl. Sci. Res.* A **1** 27–34